Received: 31 August 2021 | Revised: 12 May 2022 | Accepted: 17 August 2022

IET Power Electronics

DOI: 10.1049/pel2.12395

The Institution of Engineering and Technology WILEY

ORIGINAL RESEARCH

Simplified model predictive current control based on fast vector selection method in a VIENNA rectifier

Weizhang Song[1] | **Yang Yang**[1] | **Zhu Jiao**[1] | **Shaojie Xu**[1] | **Chaoliang Dang**[1] | **Pat Wheeler**[2]

[1]School of Electrical Engineering, Xi'an University of Technology, Xi'an, China

[2]School of Electrical and Electronic Engineering, University of Nottingham, Nottingham, UK

Correspondence
School of Electrical Engineering, Xi'an University of Technology, Xi'an, China
Email: SWZ@xaut.edu.cn

Funding information
National Natural Science Foundation of China, Grant/Award Number: 51877176; Key Research and Development Program of Shaanxi Province, Grant/Award Number: 2021GY-293; Service Local Special Plan Project of Shaanxi Provincial Education Department, Grant/Award Number: 18JC024; Xi'an Beilin District Science and Technology Plan Project, Grant/Award Number: GX2048

Abstract

This paper presents a simplified finite-control-set model predictive control (S-FCS-MPC) based on fast vector selection method in a three-level VIENNA rectifier. This method features a high-power factor, a low input current THD as a well-controlled DC-link voltage with fewer redundant vectors and lower computational load. Moreover, the converter with the proposed control technique exhibits a faster dynamic response in terms of input current and DC-link voltage compared with conventional finite-control-set model predictive control (C-FCS-MPC). In addition, the average switching frequency can be effectively reduced due to fewer switching times in a subset sector using the proposed method, which means fewer switching losses. Finally, the operation principle of the proposed algorithm has been analysed and an execution time comparison between S-FCS-MPC and C-FCS-M has been undertaken. The effectiveness of the proposed control technique has been validated using both simulation and experimental results.

1 | INTRODUCTION

Pulse width modulated (PWM) rectifiers have advantages over diode bridge rectifiers, because they feature lower input current harmonic distortion and offer a controllable power factor [1–4]. Compared to traditional unidirectional PWM rectifiers [5–7], VIENNA rectifier has many advantages, such as no dead zone for switching signal, low semiconductor device voltage stress and a simple power stage structure and control strategy [8–11]. This topology has been widely used in all-electric aircraft and wind turbine system as well as the battery charger and power factor correction system, where high-power density and low device voltage stresses are required [12–14]. However, the control scheme of VIENNA rectifier is difficult to design because of complex structure. Model predictive control (MPC) is a simple method in design and easy to multi-objective control, which is suitable for the application of VIENNA rectifier.

The finite-control-set model predictive controlhas emerged as a promising control scheme due to its advantages over conventional linear controllers, such as swift dynamic response [15] and easy inclusion of nonlinearity and system constraint [16]. Recently, this control method has been successfully applied to different power converter topologies and applications such as matrix converter and three-level inverter [17–19]. FCS-MPC undergoes no pulse-width modulation process [20], it directly selects the optimal switching state through the cost function in each control loop cycle, in order to obtain the same current waveform quality. The control loop cycle time of FCS-MPC should be substantially less than that of traditional line control method [21, 22]. However, the realization of predictive control requires significant calculation effort in each control loop cycle, especially with the rolling optimization procedure, which is a serious time-consuming process [23, 24]. This consequently poses an obstacle that impedes the application of this algorithm in three-level VIENNA rectifier.

To solve these problems, a simplification method of FCS-MPC has been proposed and discussed in [25–27]. In [25], sector distribution on a source voltage vector to reduce the

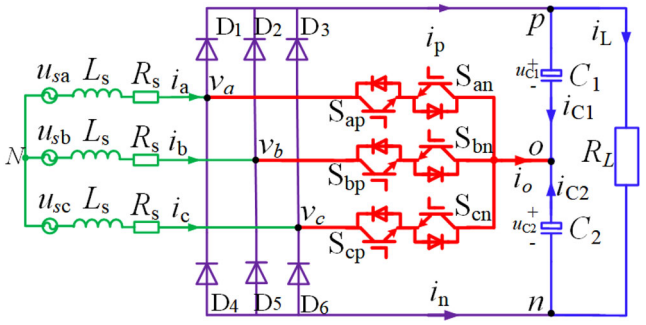

FIGURE 1 Topology of the VIENNA rectifier

number of candidate vectors in prediction process was used. Though this method reduces the program running time, the input and output performance may be affected since the selected switching vector based on this method is not the necessarily the optimal switching vector. The proposed simplified method is not completely equivalent to the original method. The method in [26] identified the optimal operating state directly from the model and the discrete number of valid states of the converter. The main advantage of this technique is that it reduces the computational cost by 43% of the algorithm that selects the best state, presenting a simple and complete algorithm without compromising the predictive control performance. In [27], a simplified two-stage model predictive control (ST-MPC) for a hybrid multilevel converter was proposed. This algorithm can dramatically reduce the computational burden and ensure the best current tracking by using a complex two-stage structure, but it is difficult to implement in engineering.

This paper presents a simplified finite-control-set model-predictive control (S-FCS-MPC) using a fast vector selection method with sector division to reduce computation time in a three-level VIENNA rectifier. This method can be implemented through the following two steps: 1) change the prediction object to reduce the predictive computational load; 2) reduce the control set in each control loop cycle by means of sector division with a subset sector. Through the above two steps, the computation time of the model predictive control will be significantly reduced, which is greatly beneficial to practical application. Noteworthily, model predictive control will lead to irregular switching action of the semiconductor switches, thus increasing the number of switching operations seriously and leading to extra switching losses [28]. In view of this issue, the presented method in this paper can shorten the number of switching operations effectively and further reduce the switching losses through setting subset sector. Simulation and experiment are conducted to validate the validity of the proposed method.

2 | C-FCS-MPC IN A VIENNA RECTIFIER

VIENNA rectifier topology is exhibited in Figure 1. The switching function S_{jo} can be defined as [29, 30]:

$$S_{jo} = \begin{cases} 1 & S_{jo}\text{ off},\ u_{sj} > 0 \\ 0 & S_{jo}\text{ on} \\ -1 & S_{jo}\text{ off},\ u_{sj} < 0 \end{cases} \qquad j = a, b, c \tag{1}$$

where S_{ao} represents S_{an} and S_{ap}, S_{bo} represents S_{bn} and S_{bp}, and S_{co} represents S_{cn} and S_{cp}.

The mathematical model in α-β coordinates can be obtained as:

$$\begin{cases} L_s \dfrac{di_\alpha}{dt} = u_{s\alpha} - R_s i_\alpha - v_\alpha \\ L_s \dfrac{di_\beta}{dt} = u_{s\beta} - R_s i_\beta - v_\beta \end{cases} \tag{2}$$

where $u_{s\alpha}$ and $u_{s\beta}$ are grid voltages, i_α and i_β are grid currents, v_α and v_β are rectifier bridge arm midpoint voltages transformed from v_a, v_b, and v_c. The values of v_a, v_b, and v_c are determined by the switching states [31]. All these components are expressed by α-β coordinates except for v_a, v_b, and v_c.

Equation (2) can be discredited as:

$$\begin{cases} \dfrac{i_\alpha(k+1) - i_\alpha(k)}{T_s} = \dfrac{1}{L_s}[u_{s\alpha}(k) - R_s i_\alpha(k) - v_\alpha(k)] \\ \dfrac{i_\beta(k+1) - i_\beta(k)}{T_s} = \dfrac{1}{L_s}[u_{s\beta}(k) - R_s i_\beta(k) - v_\beta(k)] \end{cases} \tag{3}$$

where T_s is the sampling time, $T_s = t(k+1)\text{-}t(k)$, T_s is also the control loop period.

Equation (3) can be further simplified as:

$$\begin{cases} i_\alpha(k+1) = \dfrac{T_s}{L_s}[u_{s\alpha}(k) - R_s i_\alpha(k) - v_\alpha(k)] + i_\alpha(k) \\ i_\beta(k+1) = \dfrac{T_s}{L_s}[u_{s\beta}(k) - R_s i_\beta(k) - v_\beta(k)] + i_\beta(k) \end{cases} \tag{4}$$

Equation (4) is the prediction model of VIENNA rectifier which indicates that the current value of next sampling time, $i_{\alpha,\beta}(k+1)$ can be calculated by the current value $i_{\alpha,\beta}(k)$, grid voltage value $u_{s\alpha,s\beta}(k)$ and bridge arm midpoint voltage $v_{\alpha,\beta}(k)$.

In order to minimize the input current deviation between the predictive current and the reference current at every switching state, the cost function can be expressed as:

$$g^n = \left[i_\alpha^*(k+1) - i_\alpha^n(k+1)\right]^2 + \left[i_\beta^*(k+1) - i_\beta^n(k+1)\right]^2 \tag{5}$$

where $i^n{}_\alpha(k+1)$ and $i^n{}_\beta(k+1)$ are the predictive current in α-β coordinates respectively, and $i^*{}_\alpha(k+1)$ and $i^*{}_\beta(k+1)$ are the reference predictive current in α-β coordinates respectively.

TABLE 1 Switching state table of the VIENNA rectifier

Switching state	Input bridge arm voltage($v_{\alpha N}$,$v_{\beta N}$)	Switching state	Input bridge arm voltage($v_{\alpha N}$,$v_{\beta N}$)
0 0 0	$(0,0)$	1 0 1	$(U_{dc}/5,-\sqrt{3}U_{dc}/6)$
1 0 0	$(U_{dc}/3,0)$	1–1–1	$(2U_{dc}/3,0)$
0–1–1	$(U_{dc}/3,0)$	1 0–1	$(U_{dc}/2,\sqrt{3}U_{dc}/6)$
0 0–1	$(U_{dc}/6,\sqrt{3}U_{dc}/6)$	1 1–1	$(U_{dc}/3,\sqrt{3}U_{dc}/3)$
1 1 0	$(U_{dc}/6,\sqrt{3}U_{dc}/6)$	0 1–1	$(0,\sqrt{3}U_{dc}/3)$
0 1 0	$(-U_{dc}/6,\sqrt{3}U_{dc}/6)$	–1 1–1	$(-U_{dc}/3,\sqrt{3}U_{dc}/3)$
–1 0–1	$(-U_{dc}/6,\sqrt{3}U_{dc}/6)$	–1 1 0	$(-U_{dc}/2,\sqrt{3}U_{dc}/6)$
–10 0	$(-U_{dc}/3,0)$	–1 1 1	$(-2U_{dc}/3,0)$
0 1 1	$(-U_{dc}/3,0)$	–1 0 1	$(-U_{dc}/2,-\sqrt{3}U_{dc}/6)$
0 0 1	$(-U_{dc}/6,-\sqrt{3}U_{dc}/6)$	–1–1 1	$(-U_{dc}/3,-\sqrt{3}U_{dc}/3)$
–1–1 0	$(-U_{dc}/6,-\sqrt{3}U_{dc}/6)$	0–1 1	$(0,-\sqrt{3}U_{dc}/3)$
0–1 0	$(U_{dc}/6,-\sqrt{3}U_{dc}/6)$	1–1 1	$(U_{dc}/3,-\sqrt{3}U_{dc}/3)$

Finally, all equations can be merged into a comprehensive expression for C-FCS-MPC algorithm as follows:

$$\begin{cases} i_\alpha(k+1) = \dfrac{T_s}{L_s}[u_{s\alpha}(k) - R_s i_\alpha(k) - v_\alpha(k)] + i_\alpha(k) \\ i_\beta(k+1) = \dfrac{T_s}{L_s}[u_{s\beta}(k) - R_s i_\beta(k) - v_\beta(k)] + i_\beta(k) \\ g^n = \left[i^*_\alpha(k+1) - i^n_\alpha(k+1)\right]^2 + \left[i^*_\beta(k+1) - i^n_\beta(k+1)\right]^2 \\ n_{\min} = n\Big|_{\min(g)} \end{cases} \tag{6}$$

VIENNA rectifier is a three-phase/three-level topology. However, because only the midline bridge arm has full controlled switches, it cannot produce the switching states including (1.1.1) and (−1.−1.−1), which are the switching states of zero vectors in a general three-level topology. Thus, the total number of switching states in a VIENNA rectifier is $25(3^3-2=25)$. All switching states are shown in Table 1 and Figure 3a.

Combining the comprehensive expression shown in Equation (6) with all switching states in VIENNA rectifier, the current prediction model would be calculated for 25 times in each control cycle after adopting the C-FCS-MPC. Then the deviation between the reference current and the above predictive current can be obtained in every control cycle. Finally, the optimal switching states used for controlling power semiconductors of VIENNA rectifier would be selected by using the cost function through evaluating the current error. However, there is a heavy computational load because of the 25 times of prediction current calculations and comparisons in one control cycle in C-FCS-MPC.

In order to precisely control the DC and AC sides, a double closed-loop control strategy is used for C-FCS-MPC. The voltage outer loop realizes the DC side voltage regulation function, and the voltage outer loop provides a reference given for the current inner loop, which are correspond to $i^*_{\alpha\beta}(k+1)$ and $i^n_{\alpha\beta}(k+1)$ in Equation (5), respectively. The current inner loop controls the current on the AC side, so that the total input current of the system meets the requirements of the control target. The predictive and reference values are substituted into the cost function to calculate the minimum error and select the optimal switching state. The block diagram of VIENNA rectifier based on C-FCS-MPC is exhibited in Figure 2.

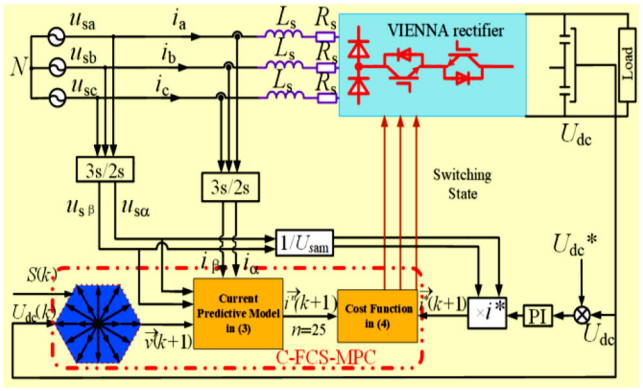

FIGURE 2 Control block diagram of C-FCS-MPC in the VIENNA rectifier

3 | S-FCS-MPC IN A VIENNA RECTIFIER

As mentioned above, the C-FCS-MPC requires 25 of times prediction current calculations in every control cycle, with 25 of times comparisons at the same time. This will increase the burden of computation, restricting the increase in the sampling frequency of the system. Thus, it is not conducive to the speedability and accuracy of the current control. To solve this problem, S-FCS-MPC based on fast vector selection method is presented in this section. The realization of this method is divided into two steps: 1) transform the predictive current at time $t(k+1)$ into other forms to shorten the computational load; 2) reduce the range of alternative vectors by reducing the control set.

3.1 | The analysis of S-FCS-MPC

Using Equation (3), a simplified expression can be derived as follows

$$\begin{cases} v_\alpha(k) = u_{s\alpha}(k) - R_s i_\alpha(k) - L_s \dfrac{i_\alpha(k+1) - i_\alpha(k)}{T_s} \\ v_\beta(k) = u_{s\beta}(k) - R_s i_\beta(k) - L_s \dfrac{i_\beta(k+1) - i_\beta(k)}{T_s} \end{cases} \tag{7}$$

In C-FCS-MPC, the optimal vectors v^n are adopted at the kth time, so at the $(k+1)$th time, the actual value of the grid current $i_{\alpha,\beta}(k+1)$ can be obtained, which is most close to the reference

value $i^*_{\alpha,\beta}(k+1)$. Replacing $i_{\alpha,\beta}(k+1)$ with $i^*_{\alpha,\beta}(k+1)$ in Equation (7), the reference voltage vector at the kth time, $v^*_{\alpha,\beta}(k)$ can be deduced as:

$$\begin{cases} v^*_\alpha(k) = u_{s\alpha}(k) - R_s i_\alpha(k) - L_s \dfrac{i^*_\alpha(k+1) - i_\alpha(k)}{T_s} \\ v^*_\beta(k) = u_{s\beta}(k) - R_s i_\beta(k) - L_s \dfrac{i^*_\beta(k+1) - i_\beta(k)}{T_s} \end{cases} \tag{8}$$

Equation (8) means that the current value $i_{\alpha,\beta}(k+1)$ at the $(k+1)$th time will be accurately equal to its reference $i^*_{\alpha,\beta}(k+1)$ as long as the voltage vector $v(k)$, which is selected at the kth time, is equal to the calculated reference voltage vector $v^*_{\alpha,\beta}(k)$.

With the above transformation, the direct prediction of the current is transformed into an indirect prediction of the current by selecting the appropriate voltage vector $v(k)$. Therefore, this simplified FCS-MPC method requires selecting one of the 25 possible voltage vectors of the VIENNA rectifier that is closest to the prediction reference $v^*(k)$. Accordingly, the new cost function is constructed as follows:

$$g^n = \left[v^*_\alpha(k) - v^n_\alpha(k)\right]^2 + \left[v^*_\beta(k) - v^n_\beta(k)\right]^2 \tag{9}$$

This method uses the one-time prediction reference voltage to substitute for 25 times of prediction of current $i_{\alpha,\beta}(k+1)$, thereby significantly reducing the computational load of a control cycle.

By analysing the operation mode of the VIENNA rectifier, only a few switching vectors will appear for each section of the three-phase grid voltage, which are the subsets of the 25 switching vectors. In order to further simplify FCS-MPC algorithm for the VIENNA rectifier, the control set can be divided into several subsets. Thus, the number of candidate vectors in each control cycle can be reduced in this way. According to the space vector distribution of VIENNA rectifier, the control set can be divided by the way of sector division. Then the switching vectors in each sector are searched for switching state table with sector division, so the traversal optimization can be carried out in this switching state subset to reduce the computational load for MPC algorithm in a three level-type VIENNA rectifier.

The operating range of VIENNA rectifier is limited due to the particularity of its structure which is of the unidirectional-boost type. For this reason, there are no redundant vectors in each sub-control set after sector division, which further reduces the number of candidate vectors. For the same reason, the switching vector of VIENNA rectifier is determined by the polarity of the grid current. In other words, there are only eight definite voltage vectors, which are determined by the eight switching states, in a certain sector, so that the candidate vectors are minimized, thereby minimizing the number of iterations and maximizing the efficiency of the algorithm.

According to the polarity of the three-phase input current, the space voltage vectors of VIENNA rectifier can be divided into six sectors as exhibited in Figure 3a. The input current polarity of the VIENNA rectifier has the same phase with the input voltage. Therefore, it is also possible to divide the sectors according to the division scheme as shown in Figure 3b. In each sector, the voltage value of one phase is greater than zero, while the other two phases are less than zero. For instance, in sector I, $v_a(k)$ is greater than zero, while $v_b(k)$ and $v_c(k)$ (where $v_a(k)$, $v_b(k)$, and $v_c(k)$ are transformed from $v^*_\alpha(k)$ and $v^*_\beta(k)$) are less than zero.

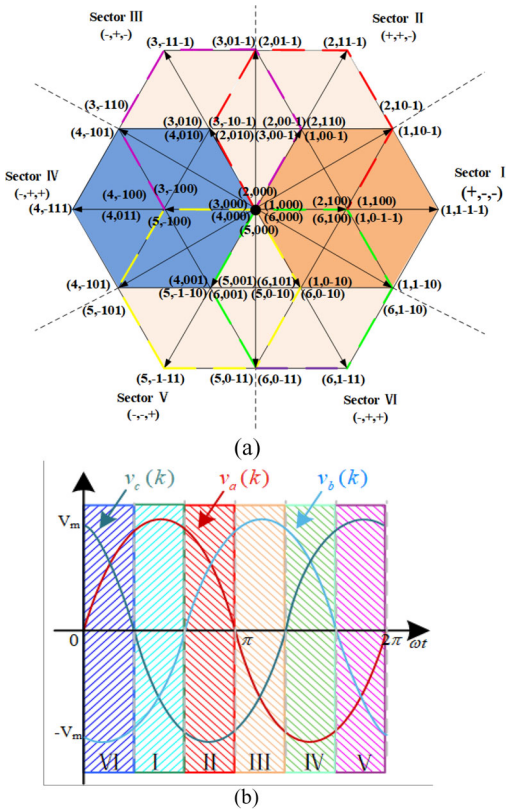

FIGURE 3 Sector definition of the VIENNA rectifier. (a) Space vector distribution diagram of VIENNA rectifier. b) Sector division diagram

The specific method of the S-FCS-MPC based on fast vector selection method is that after obtaining the reference voltage vectors $v^*_{\alpha,\beta}(k)$, inverse Clarke transform is performed to obtain $v_a(k)$, $v_b(k)$, and $v_c(k)$. The certain sector then can be determined according to the method of Figure 3b. Finally, the traversal optimization of the optimal switching vector is performed as shown in Figure 4 and the switching state table of simplified model predictive control is shown in Table 2 (with the first sector as an example).

Furthermore, the reference voltage vectors $v^*_{\alpha,\beta}(k)$ in the simplified FCS-MPC based on fast vector selection method can be obtained by using the above equations. Then, the predicted values are substituted into the cost function. The value of the cost function is compared by a simple element comparison method named enumeration [32, 33]. The minimum of the cost function and its corresponding switching state selection are obtained, which is also the most optimal switching

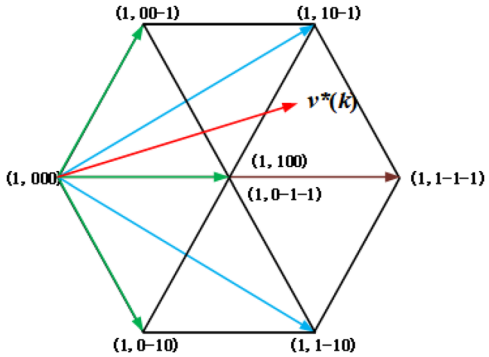

FIGURE 4 Traversal optimisation of the optimal switching vector in Sector I

TABLE 2 Switching state of the first sector and input voltage of bridge arm

Switching state	Input bridge arm voltage($v_{\alpha N}$,$v_{\beta N}$)
0 0 0	(0, 0)
0–1 0	($U_{dc}/6$, $-\sqrt{3}U_{dc}/6$)
1-1 0	($U_{dc}/2$, $-\sqrt{3}U_{dc}/6$)
1 0 0	($U_{dc}/3$, 0)
1 0–1	($U_{dc}/2$, $\sqrt{3}U_{dc}/6$)
0 0–1	($U_{dc}/6$, $\sqrt{3}U_{dc}/6$)
0–1–1	($U_{dc}/3$, 0)
1–1–1	($2U_{dc}/3$, 0)

states to be executed as gate signals for VIENNA rectifier system.

According to the reasoning above, the specific implementation steps of S-FCS-MPC based on fast vector selection with sector division can be summarized as follows:

Step 1: Sample the input current and voltage, and obtain the initial value.
Step 2: Divide the voltage space vectors into six sectors as shown in Figure 3a.
Step 3: Calculate the voltage vector $v^*_{\alpha,\beta}(k)$ for one time using Equation (8).
Step 4: Determine the sector in which the reference voltage vector is located.
Step 5: Calculate the cost function using Equation (9), and perform the traversal optimization in the order of Table 1 to find the switching state that minimizes the cost function.
Step 6: Obtain the optimal switching state and use these switching states to control the VIENNA rectifier.

All the aforementioned equations can be merged into an expression for S-FCS-MPC algorithm based on fast vector selection with sector division in a VIENNA rectifier as follows:

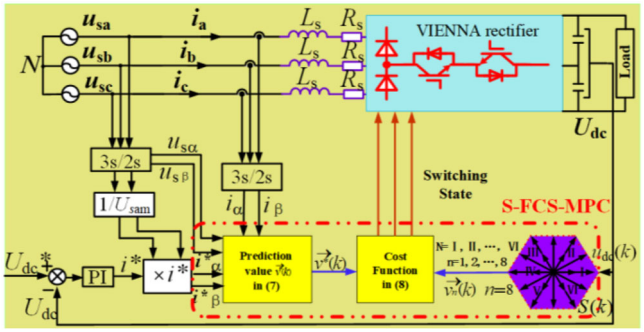

FIGURE 5 Control block diagram for S-FCS-MPC in the VIENNA rectifier

$$\begin{cases} v^*_\alpha(k) = u_{s\alpha}(k) - R_s i_\alpha(k) - L_s \dfrac{i^*_\alpha(k+1) - i_\alpha(k)}{T_s} \\ v^*_\beta(k) = u_{s\beta}(k) - R_s i_\beta(k) - L_s \dfrac{i^*_\beta(k+1) - i_\beta(k)}{T_s} \\ g^n = \left[v^*_\alpha(k+1) - v^n_\alpha(k+1)\right]^2 + \left[v^*_\beta(k+1) - v^n_\beta(k+1)\right]^2 \\ n_{\min} = n\big|_{\min(g)} \quad n = 1, \ldots, 8 \end{cases} \tag{10}$$

where the current references $i^*_\alpha(k+1)$ and $i^*_\beta(k+1)$ are determined by voltage outer loop and grid voltage together.

The voltage outer loop of S-FCS-MPC and C-FCS-MPC is PI controllers. When the PI parameters are the same, the dynamic performance of VIENNA rectifier depends on the predictive control algorithm of current inner loop. When the input current belongs to the first sector and the system load step changes, in order to maintain the stability of the output voltage, it is necessary to select the appropriate switching state to act on the power switch to ensure that the output voltage follows the given one.

From the analysis above, the block diagram of S-FCS-MPC with double loop control based on fast vector selection in VIENNA rectifier is obtained as shown in Figure 5. The PI controller is used to keep the output voltage stable in the voltage outer loop, and a simplified model predictive control is used in the current inner loop. The phase of the current reference is determined by the grid voltage, and the amplitude is determined by the output of the outer loop, which ensures the unit power factor operation of the system.

3.2 | The equivalence between S-FCS-MPC and C-FCS-MPC

The prediction model of S-FCS-MPC was transformed and the range of alternative vectors was reduced through the analysis above. Meanwhile the equivalency between the S-FCS-MPC and the C- FCS-MPC can be proved easily. A new cost function can

be obtained by substituting Equation (8) into Equation (9), and it can be further simplified as follows:

$$g^n = \left(\frac{L_s}{T_s}\right)^2 \left\{ \frac{T_s}{L_s} \left[u_{s\alpha,\beta}(k) - R_s i_{\alpha,\beta}(k) - v^n_{\alpha,\beta}(k) \right] + i_{\alpha,\beta}(k) - i^*_{\alpha,\beta}(k+1) \right\}^2 \quad (11)$$

After substituting Equation (4) into Equation (11), the cost function can be rewritten as:

$$\begin{aligned} g^n &= \left(\frac{L_s}{T_s}\right)^2 \left[i_{\alpha,\beta}(k+1) - i^*_{\alpha,\beta}(k+1) \right]^2 \\ &= \left(\frac{L_s}{T_s}\right)^2 \left[i^*_{\alpha,\beta}(k+1) - i_{\alpha,\beta}(k+1) \right]^2 \end{aligned} \quad (12)$$

From the above equations, a conclusion can be easily drawn: compared with the C-FCS-MPC, the new cost function constructed by the voltage vector model is $(L_s/T_s)^2$ times of the original cost function. There is only a difference in the coefficient between these two kinds of cost functions. Therefore, the two methods have the same performance on the control of the grid-current in VIENNA rectifier. Such an analysis verifies that the control performance of S-FCS-MPC is the same as that of C-FSC-MPC.

For S-FCS-MPC algorithm, when the input current is in the first sector, the alternative switching states are shown in Table 2. The optimal switching states selected must also be in the eight switching states shown in Table 2. Because in the first sector, the other 16 switching vectors are redundant switching vectors as determined by current polarity. According to the above analysis, compared with the C-FCS-MPC, the S-FCS-MPC algorithm does not affect the steady-state performance.

Assuming that the input voltage of the bridge arm corresponding to the optimal switching state is $(U_{dc}/6, \sqrt{3}U_{dc}/6)$, it can be seen from Table 1 that there are two corresponding switching states, (1,1,0) and (0,0,−1), respectively. Of the two switching states, (0,0,−1) is the effective and optimal switching state in the first sector, and the other is the invalid switching state. Obviously, the switching state selected randomly is not necessarily the optimal switching state in the first sector. Therefore, it can be concluded that under the C-FCS-MPC algorithm, the switching state to be selected is not the optimal switching state of the current sector. This situation, however, does not exist under the S-FCS-MPC algorithm, which means that the S-FCS-MPC algorithm has better dynamic performance than C-FCS-MPC.

3.3 | Comparison of computation time between S-FCS-MPC and C-FCS-MPC

The flow diagram of the C-FCS-MPC is exhibited in Figure 6a, and that of S-FCS–MPC is exhibited in Figure 6b. Judging from

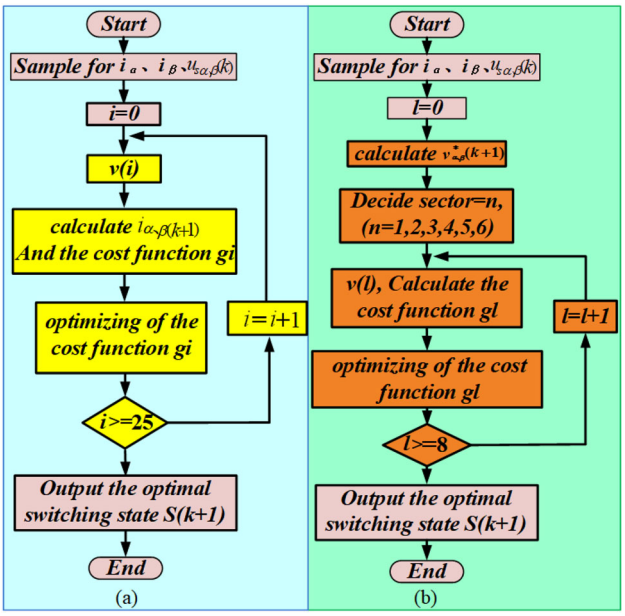

FIGURE 6 The flow diagram. (a) C-FCS-MPC and (b) S-FCS-MPC

the above implementation process, the S-FCS-MPC only needs to calculate once for the voltage vector predictive model in each control cycle, and it then compares the switching state corresponding to this voltage vector with the eight candidate vectors for eight times in every sector. Finally, the obtained optimal switching states are used to control VIENNA rectifier.

The C-FCS-MPC needs to calculate 25 times for the current predictive model in each control cycle and compare with the reference current 25 times in each control cycle. However, S-FCS-MPC only needs to calculate once and compare eight times with eight candidate vectors in each control cycle as shown in Table 3. The traversal optimization processes in Figure 6 clearly show that the S-FCS-MPC based on fast vector selection requires much fewer calculation times than the C-FCS-MPC. As mentioned above, the predictive calculation and traversal optimization of the C-FCS-MPC of the VIENNA rectifier take a lot of time. In contrast, the S-FCS-MPC reduces the computation time by dramatically reducing computational load and traversal optimization times.

4 | SIMULATION AND EXPERIMENTAL RESULTS

A simulation based on the MATLAB/SIMULINK environment was performed to validate the feasibility of the proposed S-FCS-MPC with fast vector selection in a VIENNA rectifier system. The simulation parameters are exhibited in Table 4.

According to the proposed S-FCS-MPC, selecting the output switching state between two adjacent vectors in each sector can reduce the semiconductor switching frequency, which implies fewer switching losses. When the reference voltage vector $v^*(k)$ changes in the first sector of Figure 4, the selected optimal switching state is roughly in accordance with the switching

TABLE 3 Comparison of the time consumed between by C-FCS-MPC and S-FCS-MPC

	C-FCS-MPC	S-FCS-MPC	Time consumed
Times of calculating	25 times/ each control cycle	1 times/each sector with fundamental frequency	Long (prime time-consuming)
Times of Comparing	25 times/each control cycle	8 times /each sector with fundamental frequency	Short
Time-consuming	Long	Short	

TABLE 4 System parameters

Parameter	Value
Grid-voltage(maximum value)	100 V/50 Hz
DC-link voltage reference	200 V
Load resistor	57 Ω
AC filter inductor	10 mH
DC-link filter capacitor	1650 μF(two 3300 μF/400 V series)
Sampling frequency	10 kHz
P of PI regulator	3.6
I of PI regulator	0.015
Rated power	6 kW

sequence of the first sector in Table 2. When the system enters a steady state, the number of the switching transition between the adjacent active vectors is strictly limited to one. As shown in Figure 4, when the vector is switched from (1,0−10) to (1,1−10), there is only one power switch change, and the number of the switching transition is one. Thus, the average switching frequency defined by Equation (13) controlled by the S-FCS-MPC is also reduced, which means fewer switching losses in this topology.

In order to compare the switching frequency of the semiconductor switches of the VIENNA rectifier in these two predictive control methods, the average switching frequency of the six semiconductor switches of the VIENNA rectifier is defined as follows [25]:

$$f_{re} = \frac{1}{6}\sum_{i=1}^{6} f_{re}(i) \tag{13}$$

where $f_{re}(i)$ represents the average switching frequency of the ith semiconductor switch.

Figure 7a shows the comparison between the average program execution time consumed by C-FCS-MPC and S-FCS-MPC, respectively. It can be seen that the average execution time of the S-FCS-MPC is about 1.1×10^{-5}s, while that of the C-FCS-MPC is about 2.6×10^{-5}s. In other words, the average execution time of the S-FCS-MPC algorithm is only a half of that of the C-FCS-MPC algorithm. This effective shortening of program average execution time is helpful into shortening the control cycle of the system so as to achieve precise control performance of the control target.

Figure 7b shows the comparison between the average switching frequency in C-FCS-MPC and S-FCS-MPC. The switching

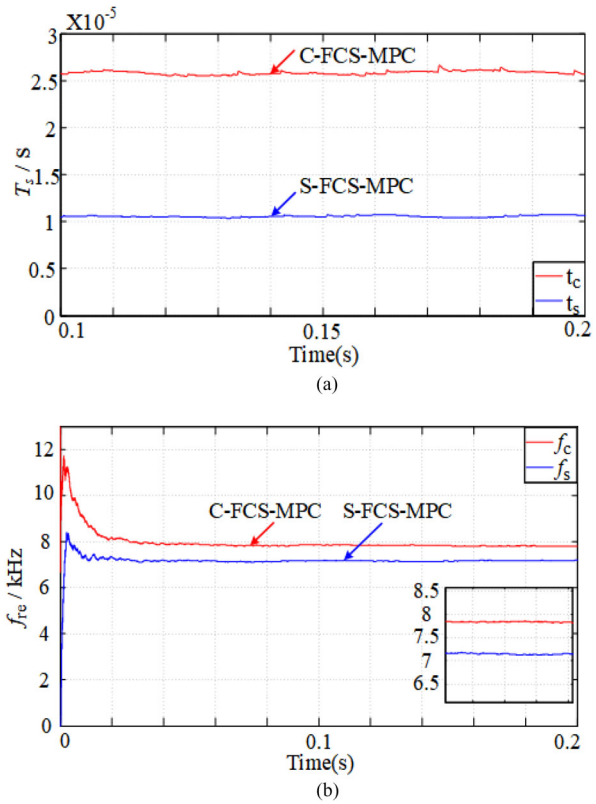

FIGURE 7 Comparison between S-FCS-MPC and C-FCS-MPC. (a) Average program execution time and (b) average switching frequency

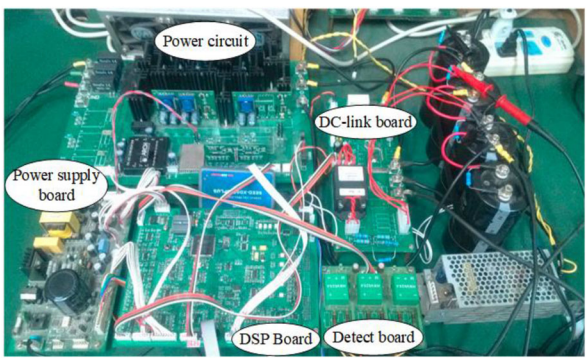

FIGURE 8 Experimental prototype

losses of power devices depend on the number of switching device operations [34] and the switching frequency [35]. Therefore, there are two main methods to reduce the loss of switching devices: (1) reducing the switching frequency, that is reducing the reduce number of switching in a single cycle [35]; (2)

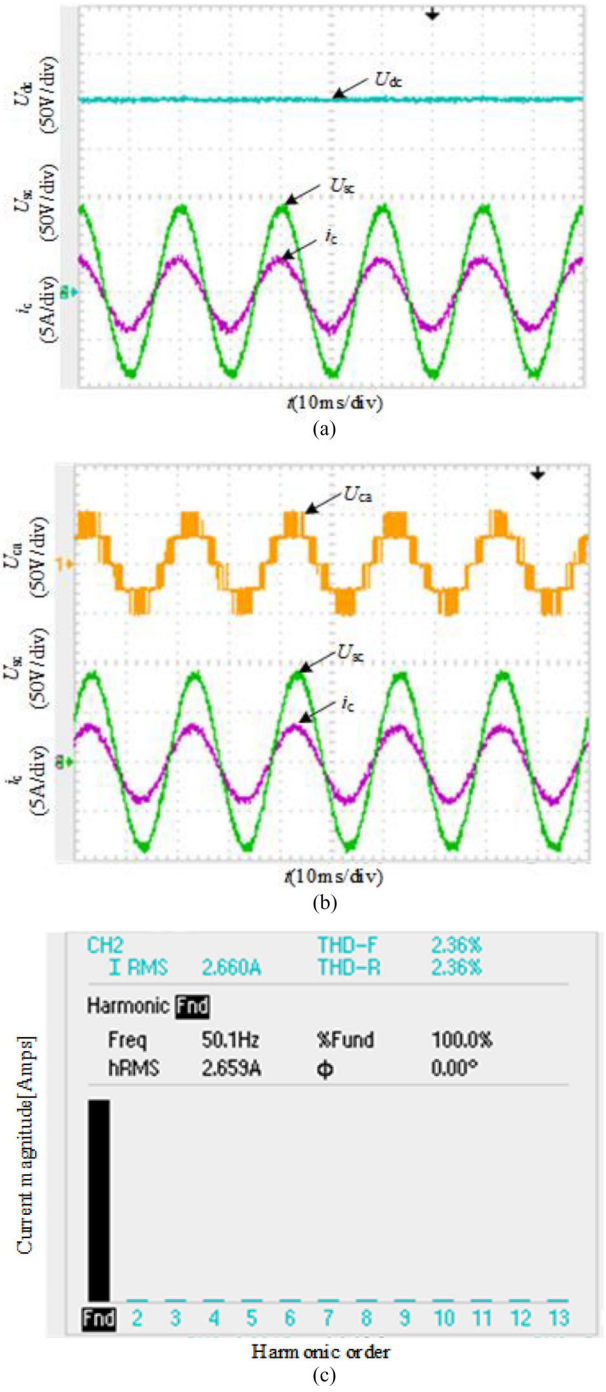

FIGURE 9 Steady-state experimental waveforms under S-FCS-MPC. (a) Input phase voltage, phase current and DC-link voltage. (b) Input phase voltage, phase current and line-to-line voltage. (c) THD analysis of input current.

changing the switching sequence in a cycle to the number of switching actions [34]. In this paper, the method of reducing the switching frequency is adopted to reduce the switching losses. It can be seen from Figure 7b that the average switching frequency of the six semiconductor switches of the VIENNA rectifier based on the S-FCS-MPC algorithm is lower than that based on the C-FCS-MPC algorithm. This proves that the

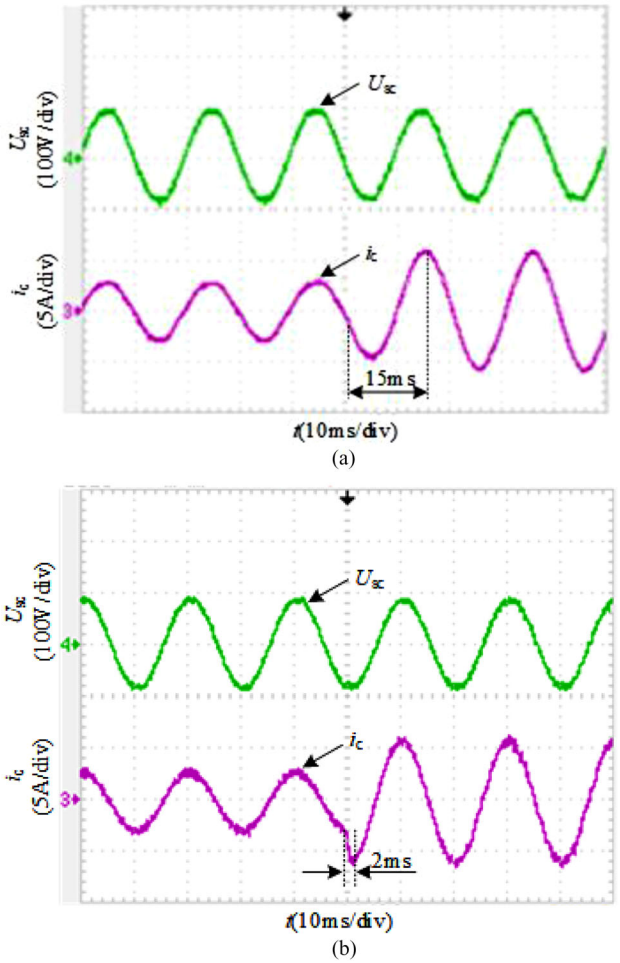

FIGURE 10 Dynamic response waveforms of given current step. (a) Input phase voltage and phase current under C-FCS-MPC and (b) input phase voltage and phase current under S-FCS-MPC

S-FCS-MPC strategy can reduce the average switching frequency, thus helping to reduce the switching losses and improve system efficiency.

A power converter prototype, as shown in Figure 8, was built to further verify the effectiveness of the proposed S-FCS-MPC. The control platform consists of a full digital signal processor (DSP) system based on TMS320F2812 and a sampling and conditioning circuit. The experimental parameters are the same as the abovementioned simulation parameters.

Figure 9 shows the input phase current, phase voltage, line-to-line voltage, DC-side voltage, and THD analysis of input current with C-FCS-MPC. Specifically, Figure 9a shows the input phase voltage, phase current, and output DC-link voltage under the S-FCS-MPC. It can be seen that the input phase current is in phase with the input phase voltage resulting in a 0.99 input power factor obtained by experimental measurement. Moreover, the output voltage is maintained constant at a set value of 200 V. Figure 9b shows the input phase voltage, phase current, and line-to-line voltage. It can be seen that the input line-to-line voltage is a five-level waveform, which verifies the multi-level feature of VIENNA rectifier. Figure 9c shows

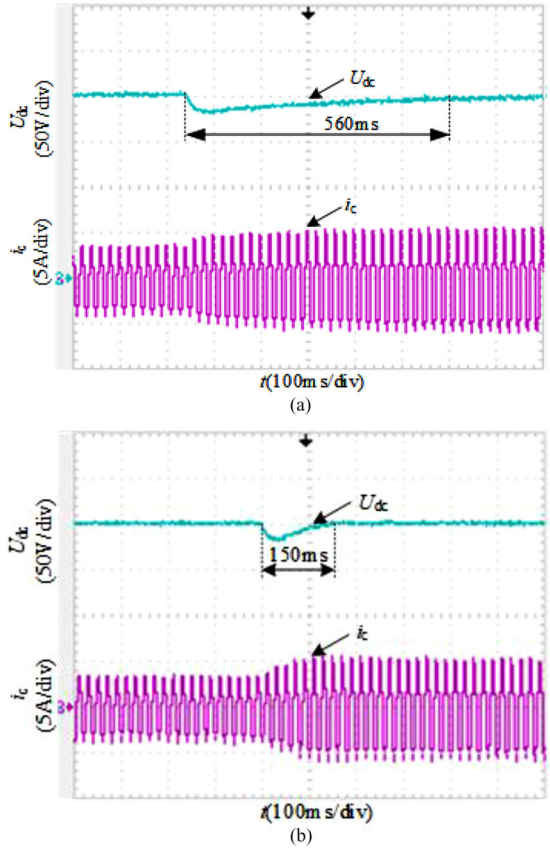

FIGURE 11 Dynamic response waveforms of DC-link voltage and input current when the load steps from 60% to 100%; (a)with C-FCS-MPC and (b) with S-FCS-MPC

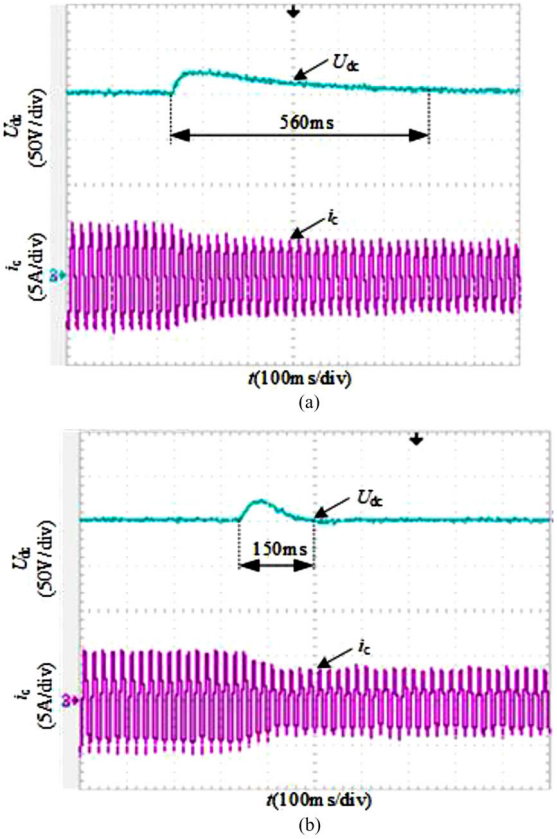

FIGURE 12 Dynamic response waveforms of DC-link voltage and input current when the load steps from 100% to 60% (a) under C-FCS-MPC, (b) under S-FCS-MPC

the harmonic analysis of input current under the S-FCS-MPC. The THD is 2.36%, which is also lower than 5% of the grid-side criterion as mentioned in [28].

Figure 10a,b shows the comparison of the dynamic response waveforms between the S-FCS-MPC and C-FCS-MPC in a VIENNA rectifier. The two control algorithms were all tested under the same condition of suddenly adding the given current value from 2.8 to 5.8 A. Comparing Figure 10a and Figure 10b, it can be seen that the input current under the C-FCS-MPC needs 15 ms to track from 2.8 to 5.8 A, whereas that under the proposed S-FCS-MPC only needs 2 ms. The comparison result confirms that the dynamic response performance in terms of the input current of the proposed S-FCS-MPC is superior to that of the C-FCS-MPC.

Figure 11 shows the dynamic response waveforms of DC-link voltage and input current between the C-FCS-MPC and the proposed S-FCS-MPC method when load steps from 60% load to 100% load. It can be seen that the DC-link voltage under C-FCS-MPC needs 560 ms to recover the set value, however, the DC-link voltage under the proposed S-FCS-MPC method only needs 150 ms to recover the set value because of the reduced calculation time under the same test condition, which steps from 60% load to 100% load. The comparison result shows that the dynamic response of S-FCS-MPC has a better performance than C-FCS-MPC.

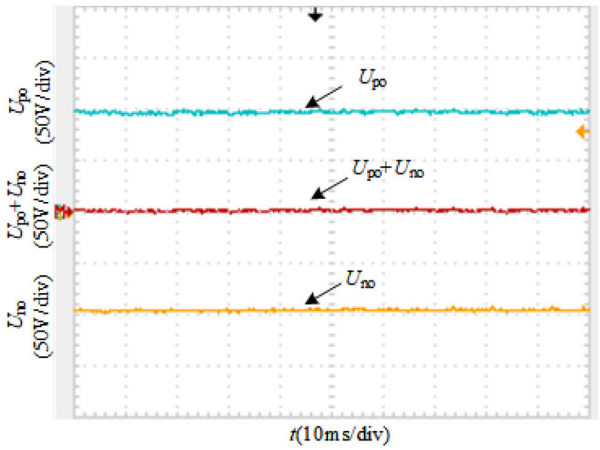

FIGURE 13 Neutral point voltage under S-FCS-MPC

Figure 12 shows the dynamic response waveforms of DC-link voltage and input current under the C-FCS-MPC and the proposed control method when load steps from 100% to 60%. It can be seen that the DC-link voltage under C-FCS-MPC needs 560 ms to return to the set value, whereas that under the proposed control method only needs 150 ms to return to the set value when load steps from 100% to 60%. The comparison results reveal that the S-FCS-MPC features a faster

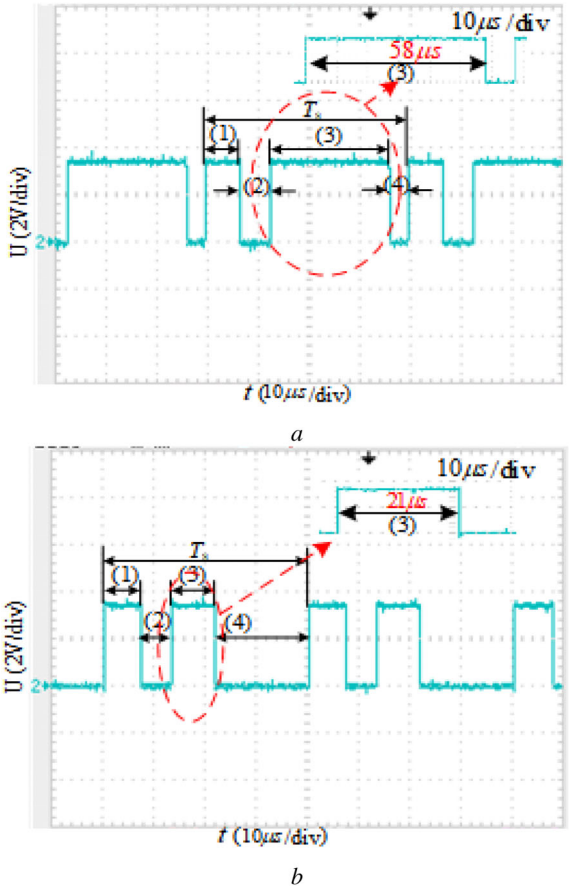

FIGURE 14 The comparison of program execution time. In the figure, (1) represents the execution time of A/D conversion, (2) represents the execution time of other programs, (3) represents the execution time of predictive calculation and traversal optimization, (4) represents the free time. (a) Execution time of C-FCS-MPC and (b) execution time of S-FCS-MPC

dynamic response than the C-FCS-MPC because of the reduced calculation time.

Figure 13 shows the neutral point voltage under S-FCS-MPC. It can be seen that the voltage amplitude U_{po} of capacitor C_1 is the same as the voltage amplitude U_{no} of capacitor C_2. And the sum of the two voltages $U_{po} + U_{no}$ is close to zero. This proves that the neutral point voltages of the two DC-side capacitors are balanced with using the proposed method.

Figure 14 shows the experimental test waveforms of the execution time for each part of the code through a GPIO output under the C-FCS-MPC and S-FCS-MPC. As can be seen from Figure 14a, in the case of a control period of 100 μs, the A/D conversion of C-FCS-MPC algorithm takes ≈17 μs, the execution time of other programs such as the voltage outer loop control takes ≈15 μs, and the prediction calculation and traversal optimization process in C-FCS-MPC takes 58 μs. As can be seen from Figure 14b, under the same conditions, the execution time of A/D conversion and other programs such as the voltage outer loop control in S-FCS-MPC is the same as that in C-FCS-MPC, but the predictive calculation and traversal optimization process in S-FCS-MPC only takes 21 μs, which is less than that C-FCS-MPC.

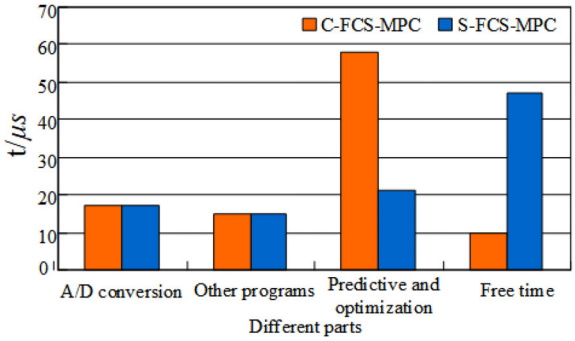

FIGURE 15 Comparison of the execution time consumed by C-FCS-MPC and S-FCS-MPC algorithms

In order to compare the difference in terms of execution time consumed by C-FCS-MPC and S-FCS-MPC clearly, the column chart which directly presents the execution time of each part of the two algorithms is shown in Figure 15. From the above comparison results of test waveforms and column chart, it can be seen that the S-FCS-MPC algorithm greatly reduces the execution time in terms of the predictive calculation and the traversal optimization compared to C-FCS-MPC, thus availably shortening its control period and further improving the control performance of this system.

5 | CONCLUSIONS

A simplified FCS-MPC based on fast vector selection method to decrease the time consumed by MPC algorithm in a VIENNA rectifier has been presented in this paper. The proposed method in a VIENNA rectifier exhibits a low input current THD, a high-power factor, as well as a constant DC-link voltage with fewer redundant vectors and calculational load. Moreover, this algorithm has featured a faster dynamic response in terms of input current and DC-link voltage compared with C-FCS-MPC. The average switching frequency has been effectively reduced due to fewer switching times in a subset sector using the proposed method, this means less switching losses. The computational load has also been effectively reduced, which makes it very suitable for practical application.

ACKNOWLEDGEMENTS

This study was supported by National Natural Science Foundation of China (51877176), Key Research and Development Program of Shaanxi Province (2021GY-293), Service Local Special Plan Project of Shaanxi Provincial Education Department (18JC024), and Xi'an Beilin District Science and Technology Plan Project (GX2048).

CONFLICT OF INTEREST

We do not have any conflict of interest.

DATA AVAILABILITY STATEMENT

The data that support the findings of this study are available from the corresponding author upon reasonable request.

REFERENCES

1. Leibl, M., Kolar, J.W., Deuringer, J.: Sinusoidal input current discontinuous conduction mode control of the VIENNA rectifier. IEEE Trans. Power Electron., 32(11), 8800–8812 (2017)
2. Adhikari, J., IV, P., Panda, S.K.: Reduction of input current harmonic distortions and balancing of output voltages of the VIENNA rectifier under supply voltage disturbances. IEEE Trans. Power Electron., 32(7), 5802–5812 (2017)
3. Leibl, M., Kolar, J.W., Deuringer, J.: Sinusoidal input current discontinuous conduction mode control of the VIENNA rectifier. IEEE Trans. Power Electron., 32(11), 8800–8812 (2017)
4. Song, W., Xing, F., Yan, H., et al.: A hybrid control method to suppress the three-time fundamental frequency neutral-point voltage fluctuation in a VIENNA rectifier. IEEE J. Emerging Sel. Top. Power Electron., 4(2), 468–480 (2016)
5. Benedetto, M.D., Lidozzi, A., Solero, L., et al.: Low-frequency state-space model for the five-level unidirectional T-rectifier. IEEE Trans. Ind. App., 53(2), 1127–1137 (2017)
6. Song, W., Zhong, Y., Zhang, H., et al.: A study of Z-source dual-bridge matrix converter immune to abnormal input voltage disturbance and with high voltage transfer ratio. IEEE Trans. Ind. Inf., 9(2), 828–838 (2013)
7. Rocha, N., Costa, A.E.L.D., Jacobina, C.B.: Parallel of two unidirectional AC-DC-AC three-leg converters to improve power quality. IEEE Trans. Power Electron., 33(9), 7782–7794 (2018)
8. Zhang, B., Zhang, C., Xing, X., et al.: Novel three-layer discontinuous PWM method for mitigating resonant current and zero-crossing distortion in VIENNA rectifier with an LCL filter. IEEE Trans. Power Electron., 36(12), 14478–14490 (2021)
9. Xu, D., Liu, K., Ran, X.: Computationally efficient optimal switching sequence model predictive control for three-phase VIENNA rectifier under balanced and unbalanced DC links. IEEE Trans. Power Electron., 36(11), 12268–12280 (2021)
10. Ma, H., Xie, Y., Shi, Z.: Improved direct power control for VIENNA-type rectifiers based on sliding mode control. IET Power Electron., 9(3), 427–434 (2016)
11. Lee, J.S., Lee, K.B.: A novel carrier-based PWM method for VIENNA rectifier with a variable power factor. IEEE Trans. Ind. Electron., 63(1), 3–12 (2016)
12. Satpathy, A.S., Kastha, D., Kishore, N.K.: VIENNA rectifier-fed squirrel cage induction generator based stand-alone wind energy conversion system. IEEE Trans. Power Electron., 36(9), 10186–10198 (2021)
13. Izadinia, A.R., Karshenas, H.R.: Current shaping in a hybrid 12-pulse rectifier using a VIENNA rectifier. IEEE Trans. Power Electron., 33(2), 1135–1142 (2018)
14. Reddy, D., Ramasamy, S.: Design of RBFN controller based boost type VIENNA rectifier for grid-tied wind energy conversion system. IEEE Access, 6, 3167–3175 (2018)
15. Rivera, M., Wilson, A., Rojas, C.A., et al.: A comparative assessment of model predictive current control and space vector modulation in a direct matrix converter. IEEE Trans. Ind. Electron, 60(2), 578–588 (2013)
16. Huang, J., Yang, B., Guo, F., et al.: Priority sorting approach for modular multilevel converter based on simplified model predictive control. IEEE Trans. Ind. Electron., 65(6), 4819–4830 (2018)
17. Gao, H., Wu, B., Xu, D.: Nine-switch AC/AC current source converter for microgrid application with model predictive control. IET Power. Electron., 10(13), 1759–1766 (2017)
18. Donoso, F., Mora, A., Cárdenas, R., et al.: Finite-Set model predictive control strategies for a 3L-NPC inverter operating with fixed switching frequency. IEEE Trans. Ind. Electron., 65(5), 3954–3965 (2018)
19. Liu, Y., Liang, W., Ge, B., et al.: Quasi-Z-source three-to-single-phase matrix converter and ripple power compensation based on model predictive control. IEEE Trans. Ind. Electron., 65(6), 5146–5156 (2018)
20. Su, D., Zhang, C., Dong, Y.: Finite-state model predictive current control for surface-mounted permanent magnet synchronous motors based on current locus. IEEE Access, 5, 27366–27375 (2017)
21. Zhang, Y., Xie, W., Li, Z., et al.: Low-complexity model predictive power control: double-vector-based approach. IEEE Trans. Ind. Electron., 61(11), 5871–5880 (2014)
22. Cortes, P., Rodriguez, J., Silva, C., et al.: Delay compensation in model predictive current control of a three-phase inverter. IEEE Trans. Ind. Electron., 59(2), 1323–1325 (2012)
23. Gong, Z., Dai, P., Yuan, X., et al.: Design and experimental evaluation of fast model predictive control for modular multilevel converters. IEEE Trans. Ind. Electron., 63(6), 3845–3856 (2016)
24. Barros, J.D., Silva, J.F.A., Jesus, E.J.A.: Fast-predictive optimal control of NPC multilevel converters. IEEE Trans. Ind. Electron., 60(2), 619–627 (2013)
25. Zhang, Y., Lin, H.: In: Simplified model predictive current control method of voltage-source inverter. In: 8th International Conference on Power Electronics - ECCE Asia, pp. 1726–1733. IEEE, Piscataway, NJ (2011)
26. Silva, J.J., Espinoza, J.R., Rohten, J.A., et al.: A novel simplified implementation of finite-set model predictive control for power converters. IEEE Access, 9, 96114–96124 (2021)
27. Li, Y., Diao, F., Zhao, Y.: Simplified two-stage model predictive control for a hybrid multilevel converter with floating H-bridge. IEEE Trans. Power Electron., 36(4), 4839–4850 (2021)
28. Abbaszadeh, A., Khaburi, D.A., Mahmoudi, H., et al.: Simplified model predictive control with variable weighting factor for current ripple reduction. IET Power Electron., 10(10), 1165–1174 (2017)
29. Song, W., Dai, Z., Xie, N., Wang, Y., Pat, W.: A Two methods for controlling three-time fundamental frequency neutral-point voltage. IET Power Electron., 12(4), 932–943 (2018)
30. Song, W., Xing, F. Yan, H., Lee, E., Lillo, D.L., Patrick, W., et al., 'A hybrid control method to suppress the three-time fundamental frequency neutral-point voltage fluctuation in a VIENNA rectifier. IEEE J. Emerging Sel. Top. Power Electron., 4(2), 468–480 (2016)
31. Zhu, W., Chen, C., Duan, S., et al.: A carrier-based discontinuous PWM method with varying clamped area for VIENNA rectifier. IEEE Trans. Ind. Electron., 66(9), 7177–7188 (2019)
32. Correa, P., Rodríguez, J., Rivera, M., et al.: Predictive control of an indirect matrix converter. IEEE Trans. Ind. Electron., 56(6), 1847–1852 (2009)
33. Karamanakos, P., Pavlou, K., Manias, S.: An enumeration-based model predictive control strategy for the cascaded H-bridge multilevel rectifier. IEEE Trans. Ind. Electron., 61(7), 3480–3489 (2014)
34. Suhel, S.M., Maurya, R.: A new switching sequences of SVPWM for six-phase induction motor with features of reduced switching losses. CES Trans. Electr. Mach. Syst., 5(2), 100–107 (2021)
35. Wang, Y., Zhang, X., Xie, Z., et al.: Model predictive direct current control of DFIG at low switching frequency. 2016 IEEE 8th International Power Electronics and Motion Control Conference, pp. 1432–1435 IEEE, Piscataway, NJ, (2016)

How to cite this article: Song, W., Yang, Y., Jiao, Z., Xu, S., Dang, C., Wheeler, P.: Simplified Model Predictive Current Control Based on Fast Vector Selection Method in a VIENNA Rectifier. IET Power Electron. 16, 436–446 (2023).
https://doi.org/10.1049/pel2.12395